NANO LETTERS

pubs.acs.org/NanoLett Letter

# Surface-Stress Induced Embrittlement of Metals

Anirudh Udupa,*,# Tatsuya Sugihara,# Koushik Viswanathan, Ronald M. Latanision, and Srinivasan Chandrasekar

Cite This: https://doi.org/10.1021/acs.nanolett.1c02887 Read Online

ACCESS | Metrics & More | Article Recommendations | Supporting Information



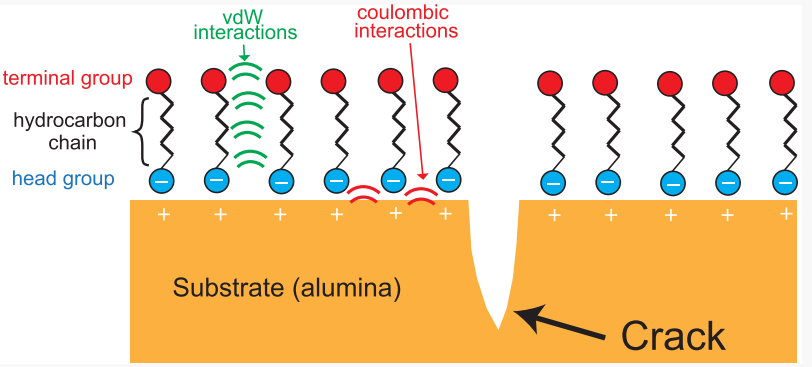


**ABSTRACT:** Environment-assisted fracture phenomena in metals are usually associated with surface energy reduction due to an adsorbed film. Here we demonstrate a unique embrittlement effect in Al that is instead mediated by surface stress, induced by an adsorbed organic monolayer. Atomistic simulations show that the adsorbate carbon-chain length $l_c$ controls the surface stress via van der Waals forces, being compressive for $l_c < 8$ and tensile otherwise. For $l_c > 8$, we demonstrate experimentally that the nanoscale film causes a ductile-to-brittle transition on the macroscale. Concomitant with this transition is a nearly 85% reduction in deformation forces. Additional simulations reveal that the microscopic mechanism for the embrittlement is via suppression of dislocation emission at incipient crack-tips. In addition to challenging long-held views on environment-assisted fracture, our findings pertaining to surface-stress induced embrittlement suggest profitable utility in manufacturing processes such as machining and comminution.

**KEYWORDS:** *Organic monolayers, ductile-brittle transition, shear deformation, surface plasticity, environment-assisted cracking*

A distinction between surface energy and surface stress sets solid surfaces apart from liquids.[1] Surface or interfacial energy, $\gamma$, is the reversible work per unit area needed to create a surface by exposing new atoms, typically by a process of cleavage.[2−5] The surface stress $f$ on the other hand is the reversible work per unit area required to stretch a surface.[2,6,7] When a liquid surface is stretched, atoms from the bulk naturally rearrange themselves to maintain constant surface density. Consequently, surface energy and surface stress (surface tension) have the same numerical value for liquids.[6] In contrast, solid surfaces can sustain elastic strains so that $f \neq \gamma$ in general. Adsorption of films on solid surfaces thus changes both $f$ and $\gamma$ simultaneously,[8] causing well-known phenomena such as surface relaxation and reconstruction.[9] Adsorption can also change the plastic deformation behavior of crystals,[10] such as in hydrogen embrittlement,[11] liquid-metal embrittlement (LME),[12] stress-corrosion cracking,[13−15] and the Bangham effect.[16]

Recently, another related, adsorbate-induced mechanochemical effect has been reported in large-strain deformation of ductile metals—coating the metal surface with an organic monolayer, a nanometer-scale film, caused local embrittlement.[17] Surprisingly, this phenomenon, henceforth called organic monolayer embrittlement (OME), was found to be critically dependent on the size of the adsorbate molecule.

It is common to attribute such film-induced embrittlement effects in metals to reduction in $\gamma$, and hence critical stress for crack growth, due to adsorption.[12,18−20] However, this thesis is insufficient to explain OME for two main reasons. First, the nanoscale organic molecule film cannot lower $\gamma$ of the material immediately ahead of a crack, because of lack of a suitable diffusion path for the molecules into the material on practically relevant time scales. Second, and more importantly, typical reductions in $\gamma$ are usually not large enough to cause

Received: July 27, 2021
Revised: October 28, 2021

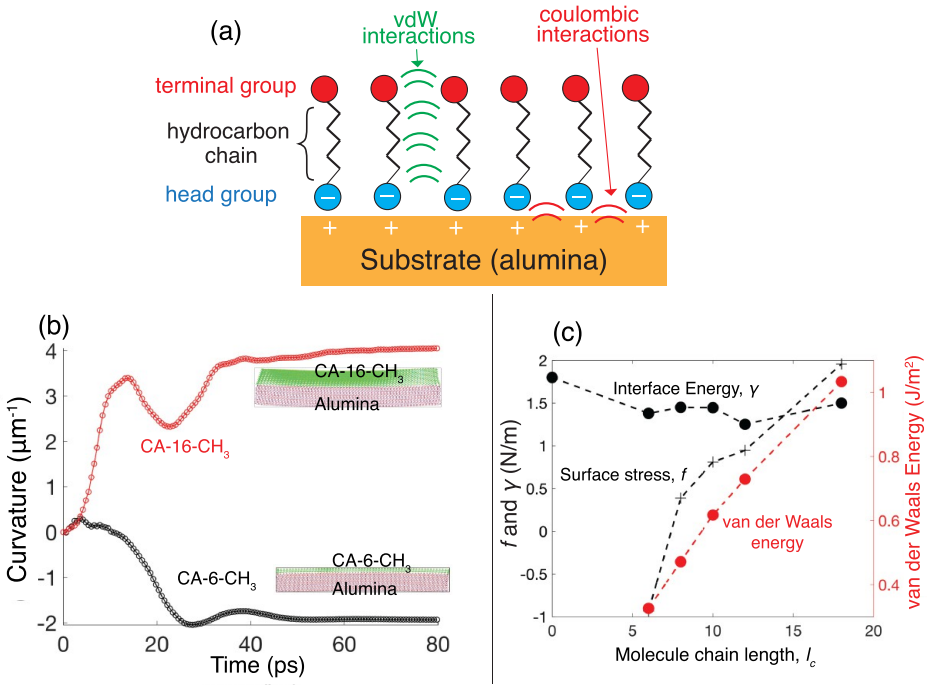


**Figure 1.** MD simulation of effects of chain length, $l_c$, on $f$ and $\gamma$. (a) Organic molecules adsorbed onto the top-side of a free-standing $Al_2O_3$ substrate (beam), showing the headgroup, hydrocarbon chain, and terminal group. The molecules experience Coulombic and van der Waals (vdW) forces. (b) Plot of substrate curvature as it equilibrates under adsorbate-induced forces. The curvature is negative (convex) for the short-chain molecule and positive for the long-chain molecule (tensile). (c) $f$ and $\gamma$ (left axis), and vdW energy (right axis, red), as a function of $l_c$.

embrittlement.[21] The other possibility, that changes in $f$ due to an adsorbate can promote crack initiation and, by extension, cause surface embrittlement, appears to have been first proposed by Oriani.[22] Unfortunately, the inability to systematically change only one of $f$ or $\gamma$ has hitherto prevented full evaluation of this hypothesis.

In this work, we show, first, using molecular dynamics (MD) simulations, that varying the size of the adsorbate molecule strongly influences $f$ while maintaining $\gamma$ constant. This immediately suggests an experimental approach for exploring the relative roles of $f$ and $\gamma$ in influencing surface plasticity and fracture in metals. Second, by creating adsorbed organic monolayer films on metal surfaces by molecular self-assembly, we show experimentally how an increased $f$ leads to embrittlement, thereby providing a fundamental basis for explaining OME and related phenomena.

The configuration used in the molecular dynamics simulations to calculate $f$, similar to a commonly used experimental setup,[23−25] consists of a microcantilever (made of $\alpha$-$Al_2O_3$, 25 nm × 5 nm × 4 nm), with an adsorbed film on one side. The $\alpha$-$Al_2O_3$ represents the native oxide layer typically present on Al surfaces, and onto which the organic monolayer is adsorbed. The cantilever deflection due to adsorption is used to calculate $f$ via Stoney's equation;[26] see Figure 1(a). Tensile (compressive) stresses arise if the deflection is concave (convex) on the adsorbate side (see Supporting Information for details). The adsorbate films were carboxylic acids (CA) with headgroup −COOH and terminal group $-CH_3$ and were self-assembled on the $Al_2O_3$ substrate. We notationally denote this class of adsorbates as CA-X-$CH_3$, explicitly indicating the headgroup (CA), chain length (X = $l_c$), and terminal group ($CH_3$). This choice is motivated by subsequent experiments that demonstrate OME in ductile Al with its native oxide layer.

The curvature evolution due to self-assembly is shown in Figure 1(b) for CA-6-$CH_3$ and CA-16-$CH_3$. At equilibrium, the cantilever has a curvature of $-2$ $\mu m^{-1}$ (CA-6-$CH_3$) and +4 $\mu m^{-1}$ (CA-16-$CH_3$), resulting in compressive and tensile $f$, respectively. These simulations were repeated for $l_c$ = 6, 8, 10, 12, and 16 and corresponding $f$ values are shown in Figure 1(c) (black-dashed line). $f$ increases monotonically with $l_c$, going from −0.96 N/m (CA-6-$CH_3$) to 1.98 N/m (CA-16-$CH_3$). We also estimated the interface energy $\gamma$ between the organic molecules and the substrate, as the difference of system energies before and after bonding. Without any adsorbate on the surface, $\gamma$ for alumina is 1.85 N/m and decreases to $\gamma \sim 1.4$ N/m with the adsorbed film, and apparently independent of $l_c$; see Figure 1(c). This is understandable, since $\gamma$ is determined primarily by the bonding of the headgroup (−COOH) with the substrate.

The reason for the observed increase of $f$ with $l_c$ is because of a competition between electrostatic interactions at the $Al_2O_3$-adsorbate interface and the van der Waals (vdW) attraction between adsorbate molecules. Charge transfer between headgroup and substrate leads to an $l_c$-independent electrostatic repulsion, contributing to a compressive surface stress. On the other hand, the red curve in Figure 1(c) shows that the magnitude of the vdW attraction per molecule increases with $l_c$, going from 0.3 J/mm$^2$ or 0.4 eV/molecule (CA-6-$CH_3$) to 1.1 J/m$^2$ or 1.35 eV/molecule (CA-16-$CH_3$). Thus, as the molecule size increases, the vdW forces eventually supersede the electrostatic repulsion contribution, making the overall surface-stress tensile. Interestingly, an analogous interaction is also responsible for the well-known monotonic increase in boiling point with $l_c$ in a homologous organic series,[27] pointing to the significant strength of this interaction.

The calculations show that by varying $l_c$, it is possible to systematically change $f$ while keeping $\gamma$ constant, thus


https://doi.org/10.1021/acs.nanolett.1c02887
Nano Lett. XXXX, XXX, XXX−XXX

suggesting a controlled method to probe the origins of OME-type phenomena. To this end, we used molecular self-assembly to deposit different alkanosilane molecules (silane headgroup) with $l_c$ between 0 and 16, on an annealed Al surface (see the Supporting Information for details). Analogous to the earlier notation, these molecules are denoted Sil-X-$CH_3$, with Sil for the silane headgroup, X = $l_c$, and the same terminal group ($CH_3$). Relevant physical properties of the adsorbate films and adsorbate-coated substrates were characterized. The thickness of the adsorbed films was measured using ellipsometry; see the blue curve in Figure 2. The average thickness changes from

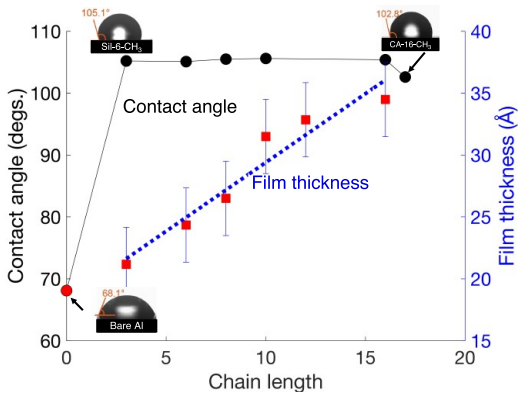


**Figure 2.** Characteristics of monolayers deposited on the Al surface. (Left axis) Contact angle from measurements with deionized water and (right axis) adsorbate-film thickness from ellipsometry.

10.6 Å (Sil-4-$CH_3$) to 27.0 Å (Sil-16-$CH_3$), typical of monolayers. In addition, contact angle measurements, before and after coating the Al substrate gave 68.1° (uncoated) and ~106° (silane-coated); see the black curve in Figure 2. The inset images show the corresponding drop configurations. The contact angles are also independent of $l_c$, as expected. The microhardness of the Al samples, with and without the adsorbates, was measured using Vickers indentation (10 g force load). Ten samples were measured for each adsorbate condition. The average hardness, across all the samples, was 25.4 ± 1.3 HV. The hardness did not show any dependence on $l_c$, or even on the presence/absence of the organic monolayers (annealed Al hardness = 24.6 HV).

The OME was experimentally evaluated by subjecting a thin surface layer of the coated/uncoated Al substrates to 2D shear deformation; see Figure 3(a) and the Supporting Information for details. High-resolution *in situ* imaging and concurrent force measurements (parallel to $V_0$) were used to analyze the deformation by evaluating strain fields, mapping flow patterns, and tracking potential fracture events. This framework provides an explicit demarcation between ductile and brittle deformation—the former if extensive plastic deformation is observed and the latter if periodic fracture events are recorded, accompanied by a reduction in force.

The time-dependent deformation force is shown in Figure 3(b) for five different Al workpieces: bare (blue), two short-chain organic monolayer (Sil-3-$CH_3$ and Sil-6-$CH_3$), and two long-chain organic monolayer adsorbates (Sil-10-$CH_3$ and Sil-16-$CH_3$). The first three cases are practically indistinguishable, the force rising gradually from zero to a maximum of ~420 N near the steady state. In addition, after ~6 s of deformation, small oscillations appear in the force trace due to tears that were seen to form in the wake of the wedge. Similar large forces were seen with all of the monolayers with $l_c \leq 6$. In dramatic contrast, with the long-chain molecules ($l_c > 8$), the deformation force is ~70 N, an approximately 85% decrease relative to the bare and short-chain cases. Moreover, the force is relatively constant during the entire deformation process, reaching steady state within 1 s of deformation imposition. This type of small (constant) deformation force was observed

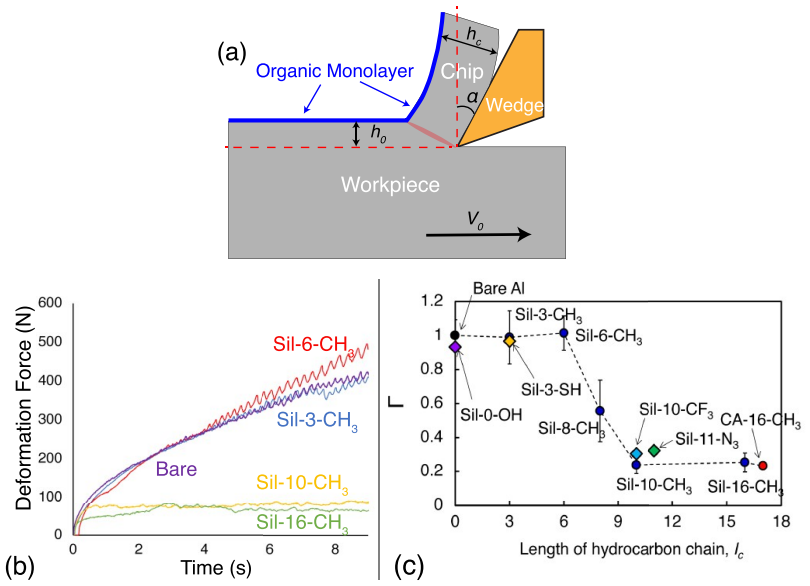


**Figure 3.** Simple-shear deformation to study effect of $l_c$ on plastic flow and embrittlement. (a) Experimental configuration: annealed Al workpiece coated with organic monolayer (blue) and experimental parameters $h_0$, $\alpha$, and $V_0$. (b) Measured deformation force for bare workpiece (blue), workpiece with short-chain adsorbates (Sil-3-$CH_3$ and Sil-6-$CH_3$), and workpiece with long-chain adsorbates (Sil-10-$CH_3$ and Sil-16-$CH_3$). The large force decrease with the long-chain molecule suggests embrittlement. (c) Plot of nondimensional force parameter ($\Gamma$) as a function of $l_c$. The data from adsorbates with silane (Sil) headgroup and $CH_3$ terminal group (Sil-X-$CH_3$) are blue circles. Data for other short- and long-chain monolayers shown as diamonds: Sil-0-OH (purple), Sil-3-SH (yellow), Sil-10-$CF_3$ (blue) and Sil-11-$N_3$ (green).



https://doi.org/10.1021/acs.nanolett.1c02887
Nano Lett. XXXX, XXX, XXX−XXX

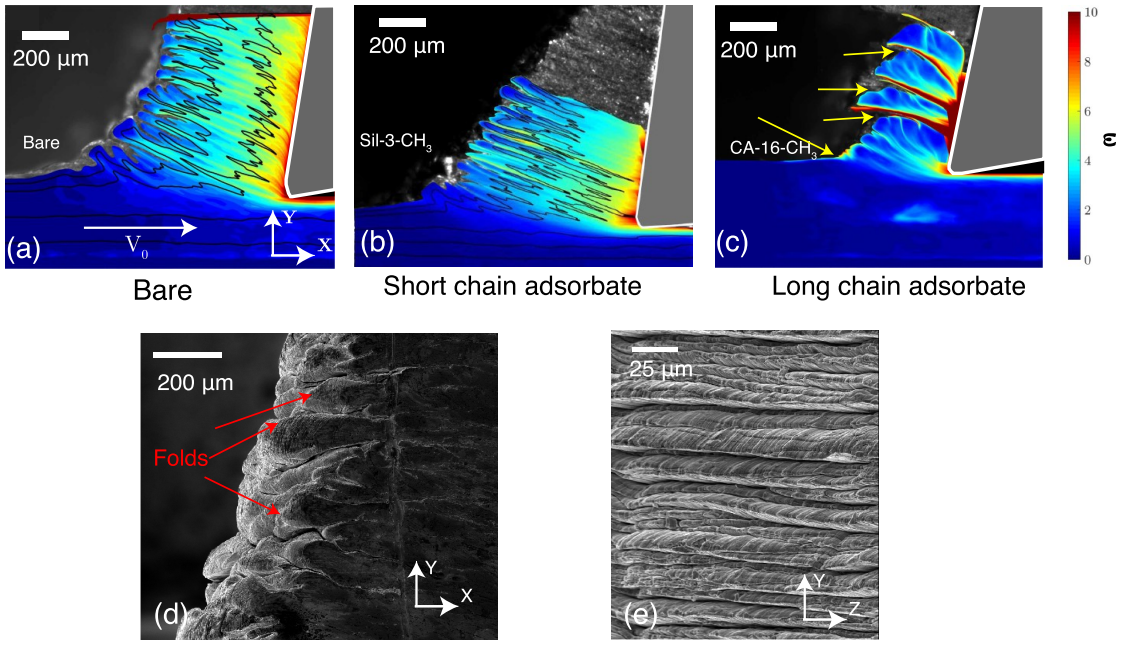


**Figure 4.** Effect of adsorbate-induced surface stress on shear deformation of Al. Top row: Single frame each from high-speed image sequences of the shearing and plastic flow: (a) without adsorbate, (b) with short-chain adsorbate (Sil-3-$CH_3$, *f* compressive), and (c) with long-chain adsorbate (Sil-16-$CH_3$, *f* tensile). In (a) and (b), the plastic deformation is severe and highly unsteady, while in (c), the flow is interrupted by quasi-periodic fracture events emanating at the free surface (yellow arrows), with much smaller strains. Bottom row: SEM images of the deformed chip: (d) without adsorbate leading to folds (red arrows) on a chip-free surface indicative of redundant plastic deformation and (e) the long-chain adsorbate case (CA-16-$CH_3$) with cracks running across the width of the chip that correspond to the quasi-periodic fractures in (c).

with all of the $l_c > 8$ monolayers, pointing to a severe disruption of surface plastic flow, potentially, via onset of a fracture instability—the OME phenomenon.

The effect of $l_c$ is highlighted in Figure 3(c) using a nondimensional parameter $\Gamma \in (0, 1]$, defined as the ratio of maximum deformation force with the monolayer to maximum force without any film. The ∼85% reduction for Sil-16-$CH_3$ corresponds to $\Gamma \approx 0.15$ in Figure 3(c). Hence $\Gamma$ is an indicator of embrittlement, with $\Gamma \ll 1$ indicating that the surface is embrittled and $\Gamma = 1$ has no effect. Figure 3(c) includes force data not only from the Sil-X-$CH_3$ molecules (blue circles) but also from other assorted short/long-chain monolayers. The latter force data include Sil-0-OH (purple diamond), a molecule with a terminal −OH group directly attached to the silane headgroup, and Sil-3-SH, Sil-10-$CF_3$, and Sil-11-$N_3$ molecules, shown as yellow, blue, and green diamonds, respectively, in the figure. There are also data for a molecule with a different headgroup (−COOH)—CA16-$CH_3$ (red circle)—corresponding to the molecule system studied in the simulations. The overwhelming conclusion from Figure 3(c) is that $\Gamma \sim 1$ when $l_c \leq 6$, transitioning to $\Gamma \sim 0.15$ for $l_c > 8$. Figure 3(c) also shows that the effect of the monolayer headgroup and terminal group on the force is secondary (if any) in comparison to the chain length.

Exactly how OME comes about is revealed by high-speed *in situ* imaging observations of material flow. The top row of Figure 4 shows one frame each from three high-speed image sequences: with bare Al workpiece (**4a**) and Al with short-chain organic monolayer (Sil-3-$CH_3$, **4b**) and long-chain organic monolayer (CA-16-$CH_3$, **4c**). Material flow is represented in these images by superimposed virtually computed streaklines[a] on a background plastic strain field (color). With the bare workpiece, a thick chip forms ($h_c/h_0 \sim 25$) due to severe plastic deformation during the shearing process. The wavy streaklines and nonhomogeneous strain field imply that the deformation field is additionally highly unsteady, with significant redundant components (rotation, material folding); see also Figure 4(d) and Supplementary Movie 1. The corresponding von Mises plastic strain in the deformed chip varies between 3.5 and 7. There is also no visible evidence of any fracture, only plastic folding in the deformed material, as further confirmed by metallography (Figure 4d). This type of unsteady, mesoscale flow, common in simple shearing of very ductile metals and called sinuous flow,[28] was also seen in workpieces with $l_c \leq 6$ (see Figure 4(b)). The extreme redundant straining accompanying the sinuous flow is responsible for large deformation forces (∼420 N) in both the bare and short-chain cases; cf. Figure 3(b).

A fundamentally different surface plastic flow mode is seen with $l_c > 8$, see Figure 4(c). First, a much thinner chip is formed, $h_c/h_0 \sim 8$; cf. Figure 4 panels (a) and (b), indicating that the extent of plastic deformation is now much reduced. Second, and most importantly, the peeled chip has a fundamentally different, "segmented" morphology, due to quasi-periodic fracture events that nucleate on the free surface (yellow arrows, Figure 4(c)) and propagate toward the wedge tip, see also Supplementary Movie 2. Once nucleated, the propagation of the crack into the material bulk is driven by the enhanced loading due to the advancing wedge (usui). The strain rate at the crack tip during the propagation was ∼80 $s^{-1}$ ($V_0$ = 5 mm/s), as measured using digital image correlation analysis. This type of crack propagation from the free surface was observed even at higher deformation speeds, $V_0$ = 1 m/s (strain rate ∼$2 \times 10^4$ $s^{-1}$), with the long-chain adsorbates. The quasi-periodic fractures manifest as cracks that run across the width of the chip-free surface; see Figure 4(e). This type of surface fracturing was observed not just with CA-16-$CH_3$ but with all $l_c > 8$, providing clear evidence that the organic


https://doi.org/10.1021/acs.nanolett.1c02887
Nano Lett. XXXX, XXX, XXX−XXX

monolayers have embrittled the surface leading to disruption of surface plastic flow. Other observations pertaining to the long-chain molecule cases, typified by Figure 4(c), are that the peeled layer is composed of trapezoidal segments separated by fracture regions; the strain within each segment being small (<2), compared to the bare and shorter-chain cases. Consequently, the deformation force is also very small ~70 N.

The dislocation mechanism that causes ductile and brittle behavior in crystalline solids has been explained by Rice and Thomson by examining what happens in the vicinity of an incipient notch in the material.[29] A loaded sharp notch in ductile materials typically self-blunts by dislocation emission, while in brittle materials, cleavage and crack propagation result. Even though the Rice−Thomson model applies to quasi-static loading, we use an analogous picture to explain the onset of crack growth in the presence of an adsorbate-induced surface stress. Once crack propagation begins, the loading field changes dynamically due to the advancing wedge and leads to continued crack growth (cf. Figure 4). To fully simulate this situation, we revert to molecular dynamics simulations of crack initiation and growth in the presence of a suitable surface stress. Figure 5 shows MD simulations of a notched Al

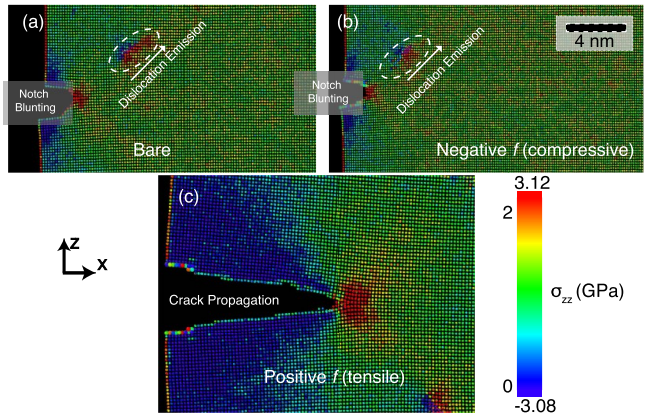


**Figure 5.** Atomistic simulations of notch behavior in the Al subject to remote tensile loading in the *Z*-direction, with and without adsorbates, and with various $f$ levels at the notch tip: (a) no adsorbate, i.e., bare Al, (b) with adsorbate $f$ = −0.6 N/m representative of short-chain monolayer, and (c) with adsorbate $f$ = 0.4 N/m representative of a long-chain monolayer. In (a), and (b), dislocation (white dotted lines) emission blunts the notch tip (ductile), while in (c), the notch cleaves (brittle). Adsorbate atoms are shown as spheres with a 20% larger radius than the Al atoms. Colors represent stress levels within the sample.

specimen, loaded remotely in tension; see Figure 5. Adsorbates are mimicked by a single atomic layer on the crack faces and suitable surface stresses realized by tuning the lattice mismatch between this layer and the substrate (see Supplementary for details). The adsorbate atoms are depicted with larger spheres than the Al atoms. Atoms in the panels of Figure 5 are colored by the local stress value.

Three sets of simulations are shown in Figure 5, 1) bare Al, 2) Al with an adsorbate at the notch tip inducing compressive surface stress ($f$ = −0.6 N/m) akin to $l_c$ < 6; and 3), and 3) Al with an adsorbate at the notch tip inducing tensile surface stress ($f$ = +0.4 N/m) similar to $l_c$ > 8. The notch is loaded in tension, and the role of $f$ is clearly evident in the resulting behavior. In the absence of significant tensile surface stress, the crack tip emits dislocations, leading to self-blunting. This response, typical of ductile metals like Al, is what is seen in the case of the bare Al sample (Figure 5(a)) and those with compressive surface stress (Figure 5(b), $f$ = −0.6 N/m). Dislocation emission ($(1/2)\langle 110\rangle$) along the {110} slip plane) is clearly revealed by zones of localized stress in these panels. A corresponding movie of the deformation, provided as Supplementary Movie 3, also reveals the blunting of the initially sharp crack by repeated dislocation emission.

In contrast, samples with a tensile surface stress of $f$ = +0.4 N/m show a very different response to the loading,;see Figure 5(c). Here a crack propagates from the tip of the notch *in lieu* of dislocation emission; see also Supplementary Movie 5. This response is typical of brittle materials; however, in the present case the material is the same as before, with the only change being the presence of tensile surface stress. This type of brittle response was observed for all $f$ > 0.3 N/m. The obvious conclusion from the simulations is that, at the microscopic level, the tensile surface stress suppresses dislocation emission from the surface notch, i.e., notch-tip plasticity, leading to surface embrittlement and fracture.

The OME phenomenon observed herein has some similarities with liquid metal embrittlement (LME), such as of Al by Ga, but with important differences. Most notably OME, unlike LME, is not catastrophic, and the residual workpiece surface left behind after peeling is not embrittled, given the absence of any diffusion pathways for the organic molecules. OME is thus a benign form of embrittlement, enabled just by monolayer adsorption.

Our experimental results have established that organic monolayers with $l_c$ > 8 cause local embrittlement of the surface under simple-shear deformation, while shorter-chain monolayers do not. Given that $l_c$ affects only $f$, the embrittlement is caused by adsorbate-induced surface stress, and not chemical corrosive action or change in $\gamma$. It is intriguing, and perhaps a bit counterintuitive, that the effect of surface stress due to a single molecular layer is so clearly manifest on the macroscale. A similar mechanism could well play a critical role in other embrittlement phenomena such as stress-corrosion cracking and LME. Preliminary measurements of surface stress induced by 100−250 nm thick ink films, as well as paint coatings,[30,31] deposited on Al-foil substrates, have shown the presence of sufficiently large tensile surface stresses. More detailed measurements of adsorbate-induced surface stress in various systems planned for the near future that should throw additional light on this matter.

Apart from warranting a revisit of classical embrittlement phenomena, our results on surface-stress-induced embrittlement by adsorbed nanometer-scale films suggest opportunities for practical applications. For instance, given the central role of van der Waals' forces in determining the surface stress, one could envisage the use of tailored additives to cutting fluids and sprays, applied locally to the cutting zone, to increase the efficiency of machining and drilling processes for ductile metals. We have, in fact, begun exploring this possibility, showing very promising preliminary results with normally difficult-to-machine metals.[32] Adsorbate-induced embrittlement could also profitably be used to increase fragmentation rates in comminution processes[33−35] including for production of powders from "gummy" metals like Al, Ni, Ta, and stainless steel. Finally, the possibility of altering the surface stress by electrochemical means, to enhance metals processing as well as study surface plasticity phenomena, warrants important consideration. This idea is suggested by earlier reports of


https://doi.org/10.1021/acs.nanolett.1c02887
Nano Lett. XXXX, XXX, XXX−XXX

changes in hardness[36] and yield stress[37] due to external electrical fields. We believe that our observations open several exciting avenues for improved control of material deformation.

## ■ ASSOCIATED CONTENT

### Supporting Information

The Supporting Information is available free of charge at https://pubs.acs.org/doi/10.1021/acs.nanolett.1c02887.

Experimental and simulation details, figure of simulation of adsorption of octadecanethiol on gold substrate, and movie captions (PDF)

Bare annealed Al workpiece deformation (MP4)

Annealed Al workpiece cracking (MP4)

Atomistic simulation of a tensile test of Al (MP4)

Atomistic simulation of a tensile test of Al with an adsorbate with compressive surface stress of −0.6 N/m (MP4)

Atomistic simulation of a tensile test of Al with an adsorbate with tensile surface stress of +0.4 N/m (MP4)

## ■ AUTHOR INFORMATION


### Corresponding Author

**Anirudh Udupa** − *Center for Materials Processing and Tribology, Purdue University, West Lafayette, Indiana 47906, United States;* orcid.org/0000-0001-7948-2046; Email: audupa@purdue.edu

### Authors

**Tatsuya Sugihara** − *Department of Mechanical Engineering, Osaka University, Suita, Osaka 565-0871, Japan*

**Koushik Viswanathan** − *Department of Mechanical Engineering, Indian Institute of Science, Bangalore 560012, India*

**Ronald M. Latanision** − *Materials Science and Engineering, MIT, Cambridge, Massachusetts 02139, United States; Exponent Inc., Natick, Massachusetts 01760, United States*

**Srinivasan Chandrasekar** − *Center for Materials Processing and Tribology, Purdue University, West Lafayette, Indiana 47906, United States*

Complete contact information is available at: https://pubs.acs.org/10.1021/acs.nanolett.1c02887

### Author Contributions

#A.U. and T.S. contributed equally to this paper.


### Notes

The authors declare no competing financial interest.

## ■ ACKNOWLEDGMENTS

This research was supported in part by NSF award DMR 2104745 and DOE EERE Award DE-EE000786.

## ■ ADDITIONAL NOTE

[a]A streakline, commonly used in fluid visualization, is defined as the locus of a fixed set of material points, as they are convected during material deformation

## ■ REFERENCES


(1) Cammarata, R. C.; Sieradzki, K. Surface and interface stresses. *Annu. Rev. Mater. Sci.* **1994**, *24* (1), 215−234.

(2) Gibbs, J. W. On the equilibrium of heterogeneous substances. *Transactions of the Connecticut Academy of Arts and Sciences* **1879**, *3*, 108−248.

(3) Cahn, J. W. Surface stress and the chemical equilibrium of small crystals−I. the case of the isotropic surface. *Acta Metall.* **1980**, *28* (10), 1333−1338.

(4) Spaepen, F. Interfaces and stresses in thin films. *Acta Mater.* **2000**, *48* (1), 31−42.

(5) Berry, M. V. The molecular mechanism of surface tension. *Phys. Educ.* **1971**, *6* (2), 79.

(6) Shuttleworth, R. The surface tension of solids. *Proc. Phys. Soc., London, Sect. A* **1950**, *63* (5), 444.

(7) Cammarata, R. C. Surface and interface stress effects in thin films. *Prog. Surf. Sci.* **1994**, *46* (1), 1−38.

(8) Haiss, W. Surface stress of clean and adsorbate-covered solids. *Rep. Prog. Phys.* **2001**, *64* (5), 591.

(9) Needs, R.; Godfrey, M.; Mansfield, M. Theory of surface stress and surface reconstruction. *Surf. Sci.* **1991**, *242* (1−3), 215−221.

(10) Latanision, R. M. *Surface Effects in Crystal Plasticity*; Noordhoff: Leyden, 1977; pp 3−48.

(11) Lynch, S. P. Hydrogen embrittlement (HE) phenomena and mechanisms. In *Stress Corrosion Cracking*; Raja, V., Shoji, T., Eds.; Woodhead Publishing: Cambridge, UK, 2011; pp 90−130.

(12) Rostoker, W.; McCaughey, J.; Markus, H. *Embrittlement by Liquid Metals*; Reinhold Pub. Corp.: New York, 1960; pp 19−30.

(13) Uhlig, H. H.; Revie, R. W. *Corrosion and Corrosion Control*, 3rd ed.; Wiley: New York, 1985; pp 23−57.

(14) Suresh, S. *Fatigue of Materials*; Cambridge University Press: Cambridge, UK, 1998; pp 570−604.

(15) Sun, S.; Chen, X.; Badwe, N.; Sieradzki, K. Potential-dependent dynamic fracture of nanoporous gold. *Nat. Mater.* **2015**, *14* (9), 894−898.

(16) Gor, G. Y.; Bernstein, N. Revisiting Bangham's law of adsorption-induced deformation: Changes of surface energy and surface stress. *Phys. Chem. Chem. Phys.* **2016**, *18* (14), 9788−9798.

(17) Sugihara, T.; Udupa, A.; Viswanathan, K.; Davis, J. M.; Chandrasekar, S. Organic monolayers disrupt plastic flow in metals. *Science Advances* **2020**, *6* (51), eabc8900.

(18) Rehbinder, P. A.; Shchukin, E. D. Surface phenomena in solids during deformation and fracture processes. *Prog. Surf. Sci.* **1972**, *3*, 97−188.

(19) Petch, N. J. The lowering of fracture-stress due to surface adsorption. *Philos. Mag.* **1956**, *1* (4), 331−337.

(20) Lawn, B. *Fracture of Brittle Solids*; Cambridge University Press: Cambridge, UK, 1993; pp 1−14.

(21) Song, E. J.; Bhadeshia, H.; Suh, D.-W. Effect of hydrogen on the surface energy of ferrite and austenite. *Corros. Sci.* **2013**, *77*, 379−384.

(22) Oriani, R. On the possible role of the surface stress in environmentally induced embrittlement and pitting. *Scr. Metall.* **1984**, *18* (3), 265−268.

(23) Berger, R.; Delamarche, E.; Lang, H. P.; Gerber, C.; Gimzewski, J. K.; Meyer, E.; Güntherodt, H.-J. Surface stress in the self-assembly of alkanethiols on gold. *Science* **1997**, *276* (5321), 2021−2024.

(24) Fritz, J. Cantilever biosensors. *Analyst* **2008**, *133* (7), 855−863.

(25) Ibach, H. Adsorbate-induced surface stress. *J. Vac. Sci. Technol., A* **1994**, *12* (4), 2240−2245.

(26) Stoney, G. G. The tension of metallic films deposited by electrolysis. *Proc. R. Soc. Lond. A* **1909**, *82* (553), 172−175.

(27) Solomons, T. G.; Fryhle, C. B.; Snyder, S. A. *Organic Chemistry*; John Wiley & Sons: Hoboken, NJ, 2011; pp 53−97.

(28) Yeung, H.; Viswanathan, K.; Compton, W. D.; Chandrasekar, S. Sinuous flow in metals. *Proc. Natl. Acad. Sci. U. S. A.* **2015**, *112* (32), 9828−9832.

(29) Rice, J. R.; Thomson, R. Ductile versus brittle behaviour of crystals. *Philos. Mag.* **1974**, *29* (1), 73−97.

(30) Croll, S. G. Residual stress in a solventless amine-cured epoxy coating. *J. Coating Technol.* **1979**, *51* (659), 49−55.

(31) Konig, A. M.; Bourgeat-Lami, E.; Mellon, V.; von der Ehe, K.; Routh, A.; Johannsmann, D. Dilational laterial stress in drying latex films. *Langmuir* **2010**, *26* (6), 3815−3820.

(32) Davis, J. M.; Saei, M.; Mohanty, D. P.; Udupa, A.; Sugihara, T.; Chandrasekar, S. Cutting of tantalum: Why it is so difficult and what can be done about it. *International Journal of Machine Tools and Manufacture* **2020**, *157*, 103607.
(33) Westwood, A. R. C.; Macmillan, N. M.; Kalyoncu, R. S. Chemomechanical phenomena in hard rock drilling. *International Journal of Rock Mechanics and Mining Science* **1974**, *11* (11), A233.
(34) McMahon, B. W.; Perez, J. P. L.; Yu, J.; Boatz, J. A.; Anderson, S. L. Synthesis of nanoparticles from malleable and ductile metals using powder-free, reactant-assisted mechanical attrition. *ACS Appl. Mater. Interfaces* **2014**, *6* (22), 19579−19591.
(35) Gayko, M.; Wostefeld, B.; Wochnowski, H. Effect of sorption and reaction processes on the strength of metals and the action of sorptive dependent tribological properties on the kinetics of crushing. *Z. Phys. Chem.* **1973**, *87* (1), 83−93.
(36) Latanision, R. M.; Opperhauser, H.; Westwood, A. R. C. The influence of applied potential on the micro-hardness of zinc monocrystal electrodes: The electrocapillary effect. *The Science of Hardness Testing* **1971**, 432−439.
(37) Kramer, D.; Viswanath, R. N.; Weissmüller, J. Surface-Stress Induced Macroscopic Bending of Nanoporous Gold Cantilevers. *Nano Lett.* **2004**, *4* (5), 793−796.


https://doi.org/10.1021/acs.nanolett.1c02887
*Nano Lett.* XXXX, XXX, XXX−XXX